Supplement of Hydrol. Earth Syst. Sci., 27, 1507–1529, 2023
https://doi.org/10.5194/hess-27-1507-2023-supplement

Hydrology and Earth System Sciences
Open Access
EGU

Supplement of

Soil–vegetation–water interactions controlling solute flow and chemical weathering in volcanic ash soils of the high Andes

Sebastián Páez-Bimos et al.

Correspondence to: Sebastián Páez-Bimos (carlos.paezb@epn.edu.ec) and Veerle Vanacker (veerle.vanacker@uclouvain.be)

Soil-vegetation-water interactions controlling solute flow and chemical weathering in volcanic ash soils of the high Andes

Section S1

Table S1. Mean soil hydraulic properties

Horizon	Depth [cm]	θ_{WP}* [$cm^3\ cm^{-3}$]	θ_S* [$cm^3\ cm^{-3}$]	θ_{FC}* [$cm^3\ cm^{-3}$]	θ_{TAW}* [$cm^3\ cm^{-3}$]	K_{SAT}** [$mm\ h^{-1}$]
			CU-UR			
A	15	0.27	0.80	0.78	0.51	175.3 (2)
	25	0.25	0.69	0.67	0.42	
2A	35	0.21	0.66	0.59	0.38	15.6 (2)
	45	0.16	0.61	0.54	0.38	
	55	0.20	0.64	0.59	0.38	
2BC	65	0.19	0.64	0.57	0.37	0.5 (2)
	75	0.15	0.52	0.45	0.30	
3BC	85	0.12	0.60	0.51	0.39	1.0 (1)
	95	0.19	0.60	0.56	0.37	
			TU-UP			
A	10	0.28	0.73	0.68	0.40	12.0 (3)
	25	0.26	0.65	0.62	0.35	
2A	35	0.15	0.62	0.57	0.42	5.0 (3)
	45	0.15	0.69	0.65	0.50	
	55	0.17	0.72	0.69	0.52	
	65	0.20	0.66	0.62	0.42	
2BC	75	0.16	0.59	0.56	0.39	6.5 (3)
	85	0.17	0.49	0.46	0.29	
3BC	95	0.17	0.61	0.54	0.37	1.0 (1)

* Mean of duplicate measurements

** number in parenthesis represents the number of replicates

Table S2. Soil physical and chemical properties

	Depth [cm]	BD [$g\ cm^{-3}$]	Sand [%]	Silt [%]	Clay [%]	SOC [%]	pH [-]	CEC [$cmol_c\ kg^{-1}$]
				CU-UR				
A	15	0.43	38.72	54.11	7.12	8.79	4.93	35.03
	25	0.74	39.15	53.37	7.47	4.80	4.82	19.47
2A	35	0.94						
	45	1.05	62.91	33.13	3.95	2.98	4.62	19.47
	55	0.95						
2BC	65	1.02	39.95	53.46	6.59	1.79	4.82	8.86
	75	1.33						
3BC	85	1.21	54.72	41.16	4.1	2.03	5.04	15.76
	95	1.07						
				TU-UP				
A	10	0.73	39.37	53.44	7.17	5.61	5.05	26.23
	25	0.92	39.39	53.26	7.38	4.97	5.12	25.56
2A	35	0.96						
	45	0.75	62.8	32.75	4.44	4.97	5.18	20.67
	55	0.62						
	65	0.82						
2BC	75	1.02	49.06	45.7	5.2	1.33	5.34	5.53
	85	1.25						
3BC	95	1.09	34.9	56.82	8.25	2.84	5.41	16.16

All properties represent one measurement, except bulk density (BD) representing the mean of duplicate measurements

Table S3. Periods for fluxmeter water volume collection and laboratory analysis.

No.	CU-UR	TU-UP	Lab analysis*
1	29/03/2019 - 09/04/2019	29/03/2019 - 10/04/2019	
2	09/04/2019 - 24/04/2019	10/04/2019 - 25/04/2019	X
3	24/04/2019 - 07/05/2019	25/04/2019 - 08/05/2019	
4	07/05/2019 - 21/05/2019	08/05/2019 - 22/05/2019	X
5	21/05/2019 - 04/06/2019	22/05/2019 - 05/06/2019	
6	04/06/2019 - 18/06/2019	05/06/2019 - 19/06/2019	X
7	18/06/2019 - 02/07/2019	19/06/2019 - 03/07/2019	
8	02/07/2019 - 16/07/2019	03/07/2019 - 17/07/2019	X
9	16/07/2019 - 30/07/2019	17/07/2019 - 31/07/2019	
10	30/07/2019 - 14/08/2019	31/07/2019 - 15/08/2019	X
11	14/08/2019 - 27/08/2019	15/08/2019 - 28/08/2019	X
12	27/08/2019 - 10/09/2019	28/08/2019 - 11/09/2019	X
13	10/09/2019 - 24/09/2019	11/09/2019 - 25/09/2019	
14	24/09/2019 - 16/10/2019	25/09/2019 - 17/10/2019	X
15	16/10/2019 - 29/10/2019	17/10/2019 - 30/10/2019	
16	29/10/2019 - 12/11/2019	30/10/2019 - 13/11/2019	X
17	12/11/2019 - 26/11/2019	13/11/2019 - 27/11/2019	
18	26/11/2019 - 10/12/2019	27/11/2019 - 11/12/2019	X
19	10/12/2019 - 26/12/2019	11/12/2019 - 27/12/2019	
20	26/12/2019 - 07/01/2020	27/12/2019 - 08/01/2020	X
21	07/01/2020 - 21/01/2020	08/01/2020 - 22/01/2020	
22	21/01/2020 - 04/02/2020	22/01/2020 - 05/02/2020	X
23	04/02/2020 - 18/02/2020	05/02/2020 - 19/02/2020	
24	18/02/2020 - 03/03/2020	19/02/2020 - 04/03/2020	X

* X indicate solute concentrations laboratory analyses conducted at the MOCA platform of the Earth and Life Institute at UCLouvain.

Table S4. Initial value, ranges (in parenthesis) for soil hydraulic parameters, and fitting van Genuchten models.

Depth [cm]	θ_r [$cm^3\ cm^{-3}$]	θ_S [$cm^3\ cm^{-3}$]	α [$1\ cm^{-1}$]	n [-]	K_{SAT} [$cm\ d^{-1}$]	w_2	α_2 [$1\ cm^{-1}$]	n_2 [-]	Unimodal RMSE	Bimodal RMSE
					CU-UR					
15	0.27 (0-0.5)	0.80 (0.77-0.81)	0.004 (0.001-0.5)	1.82 (1.01-2.5)	420.8 (48-794)	0.001 (0-0.4)	0.36 (0.01-1)	8.3 (1.5-10)	0.010	0.007
25	0.25 (0-0.5)	0.69 (0.67-0.71)	0.002 (0.001-0.5)	1.31 (1.01-2.5)	420.8 (48-794)	0.01 (0-0.4)	0.33 (0.01-1)	8.6 (1.5-10)	0.016	0.016
35	0.21 (0-0.5)	0.66 (0.62-0.69)	0.002 (0.001-0.5)	1.30 (1.01-2.5)	37.4 (17-121)	0.10 (0-0.4)	0.03 (0.01-1)	10 (1.5-10)	0.029	0.022
45	0.16 (0-0.5)	0.61 (0.58-0.62)	0.005 (0.001-0.5)	1.28 (1.01-2.5)	37.4 (17-121)	0 (0-0.4)	0.01 (0.01-1)	3.1 (1.5-10)	0.018	0.018
55	0.20 (0-0.5)	0.64 (0.63-0.65)	0.002 (0.001-0.5)	1.30 (1.01-2.5)	37.4 (17-121)	0 (0-0.4)	0.01 (0.01-1)	4.6 (1.5-10)	0.023	0.016
65	0.19 (0-0.5)	0.64 (0.63-0.66)	0.001 (0.001-0.5)	1.36 (1.01-2.5)	1.2 (0.7-1.7)	0.10 (0-0.4)	0.03 (0.01-1)	10 (1.5-10)	0.023	0.007
75	0.15 (0-0.5)	0.52 (0.50-0.55)	0.001 (0.001-0.5)	1.56 (1.01-2.5)	1.2 (0.7-1.7)	0.16 (0-0.4)	0.03 (0.01-1)	3.5 (1.5-10)	0.020	0.011
85	0.12 (0-0.5)	0.60 (0.57-0.63)	0.004 (0.001-0.5)	1.46 (1.01-2.5)	2.4 (2.4)	0.14 (0-0.4)	0.03 (0.01-1)	10 (1.5-10)	0.027	0.026
95	0.19 (0-0.5)	0.60 (0.58-0.62)	0.002 (0.001-0.5)	1.69 (1.01-2.5)	2.4 (2.4)	0.13 (0-0.4)	0.01 (0.01-1)	10 (1.5-10)	0.017	0.017
					TU-UP					
10	0.28 (0-0.5)	0.73 (0.71-0.74)	0.002 (0.001-0.5)	1.33 (1.01-2.5)	28.8 (2-70)	0.001 (0-0.4)	0.01 (0.01-1)	4.5 (1.5-10)	0.015	0.015
25	0.26 (0-0.5)	0.65 (0.61-0.68)	0.001 (0.001-0.5)	2.40 (1.01-2.5)	28.8 (2-70)	0.08 (0-0.4)	0.024 (0.01-1)	10 (1.5-10)	0.027	0.020
35	0.15 (0-0.5)	0.62 (0.57-0.66)	0.001 (0.001-0.5)	2.24 (1.01-2.5)	12.0 (6-77)	0.09 (0-0.4)	0.028 (0.01-1)	9.5 (1.5-10)	0.031	0.028
45	0.15 (0-0.5)	0.69 (0.68-0.69)	0.005 (0.001-0.5)	1.34 (1.01-2.5)	12.0 (6-77)	0.04 (0-0.4)	0.003 (0.01-1)	10 (1.5-10)	0.008	0.008
55	0.17 (0-0.5)	0.72 (0.69-0.74)	0.001 (0.001-0.5)	2.83 (1.01-2.5)	12.0 (6-77)	0.04 (0-0.4)	0.034 (0.01-1)	5.9 (1.5-10)	0.028	0.027
65	0.20 (0-0.5)	0.66 (0.63-0.68)	0.001 (0.001-0.5)	1.90 (1.01-2.5)	12.0 (6-77)	0.14 (0-0.4)	0.016 (0.01-1)	2.2 (1.5-10)	0.016	0.013
75	0.16 (0-0.5)	0.59 (0.55-0.63)	0.001 (0.001-0.5)	1.90 (1.01-2.5)	15.6 (9-38)	0.06 (0-0.4)	0.026 (0.01-1)	10 (1.5-10)	0.022	0.020
85	0.17 (0-0.5)	0.49 (0.47-0.50)	0.009 (0.001-0.5)	1.19 (1.01-2.5)	15.6 (9-38)	0.49 (0-0.4)	0.01 (0.01-1)	10 (1.5-10)	0.013	0.011
95	0.17 (0-0.5)	0.61 (0.57-0.65)	0.002 (0.001-0.5)	1.41 (1.01-2.5)	2.4 (2.4)	0.10 (0-0.4)	0.017 (0.01-1)	10 (1.5-10)	0.023	0.020

Table S5. First order (S_1) and total effect (S_T) Sobol's sensitivity indices for the 20th most sensitive soil hydraulic parameters (in decreasing order) representing all depths based on KGE function

CU-UR						TU-UP					
Parameters	Depth [cm]	S_1	Parameter	Depth [cm]	S_T	Parameters	Depth [cm]	S_1	Parameter	Depth [cm]	S_T
n	**15**	**0.079**	**n**	**35**	**0.324**	**K_{SAT}**	**10**	**0.252**	**K_{SAT}**	**10**	**0.638**
n	**65**	**0.072**	**n**	**15**	**0.312**	**n**	**10**	**0.071**	**n**	**10**	**0.47**
n	**85**	**0.053**	**n**	**25**	**0.262**	**α**	**10**	**0.069**	**α**	**10**	**0.442**
K_{SAT}	15	0.046	θ_r	25	0.26	θ_r	10	0.046	**w_2**	**10**	**0.349**
w_2	15	0.045	θ_r	15	0.229	A	85	0.039	**α_2**	**10**	**0.334**
θ_r	35	0.045	A	15	0.203	n_2	85	0.037	**θ_r**	**10**	**0.325**
θ_r	15	0.044	K_{SAT}	15	0.202	θ_S	75	0.033	**n_2**	**10**	**0.252**
n	55	0.044	n	65	0.198	θ_S	45	0.031	w_2	25	0.233
α_2	55	0.042	α	35	0.191	α_2	55	0.031	α	25	0.23
K_{SAT}	35	0.041	α	25	0.184	N	75	0.031	K_{SAT}	25	0.23
K_{SAT}	55	0.041	α_2	25	0.181	N	85	0.031	n	25	0.228
α	15	0.039	n	85	0.181	α	45	0.029	α2	25	0.228
n	95	0.039	n	45	0.18	α_2	65	0.029	θ_S	10	0.217
n2	15	0.038	w_2	15	0.179	K_{SAT}	75	0.026	θ_r	25	0.185
w_2	25	0.038	w_2	25	0.175	w_2	65	0.024	n	35	0.175
α	35	0.038	K_{SAT}	35	0.172	θ_r	85	0.024	α	35	0.172
θ_S	35	0.037	n	75	0.17	w_2	10	0.022	n	45	0.144
n	35	0.037	K_{SAT}	25	0.169	α	25	0.022	θ_S	25	0.140
α	65	0.037	w_2	35	0.166	n	65	0.020	α	75	0.136
K_{SAT}	65	0.037	n_2	25	0.165	w_2	35	0.020	w_2	35	0.134

Table S6. Fitted soil hydraulic parameters and standard error (Std. Error)

CU-UR			TU-UP		
Parameter	Depth [cm]	Fitted (Std. Error)	Parameter	Depth [cm]	Fitted (Std. Error)
n [-]	15	2.50 (0.09)	α [1 cm^{-1}]	10	0.028 (0.0002)
n [-]	25	1.21 (0.005)	n [-]	10	2.50 (0.04)
n [-]	35	2.50 (0.51)	K_{SAT} [cm d^{-1}]	10	4.96 (0.20)
n [-]	45	1.23 (0.003)	w_2 [-]	10	0.001 (0.0007)
n [-]	55	2.50 (0.54)	α_2 [1 cm^{-1}]	10	0.007 (0.0008)
n [-]	65	2.50 (0.61)	n_2 [-]	10	1.50 (0.19)
n [-]	85	1.26 (0.003)	α [1 cm^{-1}]	25	0.003 (0.00004)
			n [-]	25	2.23 (0.09)
			α [1 cm^{-1}]	65	0.018 (0.0007)
			n [-]	65	2.45 (0.10)
			α [1 cm^{-1}]	75	0.004 (0.0003)
			n [-]	75	2.50 (0.22)

Table S7. Comparison of aggregated daily data for soil water balance components and meteorological data for both soil profiles during dry (4 months) and wet periods (5 months)

	Dry periods (Jan. 2019; Jul.-Sep. 2019; Mar.2020; Oct.2020)		Wet periods (Apr.-May 2019; Oct.-Nov. 2019; Nov.-Dec. 2020; Feb. 2021)	
	CU-UR	TU-UP	CU-UR	TU-UP
Rainfall (P) [mm]	191.5	193.9	584.5	625.9
Actual Evapotranspiration (ETa) [mm]	331.6	134.7	239.3	176.0
Potential Evapotranspiration (ETp) [mm]	334.9	356.5	239.3	251.9
Deep Drainage (D) [mm]	60.0	123.6	75.2	354.5
Air Temperature [°C]	3.6	4.5	4.4	4.9
Relative Humidity [%]	92.8	91.8	93.8	94.1
Solar Radiation* [MJ m^{-2} d^{-1}]	15.4		12.2	
Wind Speed * [m s^{-1}]	4.2		2.6	

*Data recorded at the JTU_AWS weather station

Table S8. Biweekly solute concentrations [mg L^{-1}], total ion charge [meq L^{-1}] and ionic balance [%]. Mean ± Standard Deviation (n in parenthesis). Means followed by *, **, *** indicate Mann-Whitney U-Test for significant differences by soil profile for same horizons (A and 2A only) at different significance levels ($p<0.05$, $p<0.01$, $p<0.001$).

Soil profile	CU-UR			TU-UP		
Horizon	A	2A	2BC	A	2A	3BC
DOC	47.3 ± 2.3 (11) ***	9.8 ± 0.9 (10) ***	2.9 ± 0.3 (11)	3.1 ± 0.3 (12) ***	3.9 ± 0.7 (12) ***	4.0 ± 0.4 (8)
Fe	1.0 ± 0.3 (11) ***	0.04 ± 0.00 (9) ***	< 0.01 (11)	0.01 ± 0.00 (11) ***	0.01 ± 0.00 (13) ***	0.01 ± 0.00 (8)
Al	1.7 ± 0.2 (11) ***	0.14 ± 0.01 (10) ***	0.07 ± 0.02 (11)	0.06 ± 0.01 (12) ***	0.07 ± 0.02 (13) ***	0.04 ± 0.01 (8)
K	8.3 ± 0.9 (11) ***	0.7 ± 0.1 (10)	0.4 ± 0.2 (12)	2.0 ± 1.2 (10) ***	1.0 ± 1.6 (8)	0.1 ± 0.0 (5)
Ca	4.7 ± 0.7 (11) ***	4.7 ± 0.6 (10)	2.5 ± 0.5 (11)	12.8 ± 4.0 (12) ***	5.7 ± 1.4 (11)	4.7 ± 0.3 (8)
Mg	0.8 ± 0.1 (10) ***	1.5 ± 0.2 (10)	1.8 ± 0.5 (12)	4.0 ± 1.5 (12) ***	1.9 ± 0.9 (12)	1.4 ± 0.1 (7)
Na	4.5 ± 0.3 (10) **	6.3 ± 0.5 (10) ***	5.3 ± 0.9 (12)	5.5 ± 1.1 (12) **	4.1 ± 0.7 (12) ***	5.2 ± 0.3 (8)
DSi	15.9 ± 1.6 (11)	22.3 ± 2.5 (10) ***	25.0 ± 2.2 (12)	14.8 ± 3.0 (12)	18.0 ± 1.6 (13) ***	18.6 ± 1.5 (8)
HCO_3^-	31.1 ± 4.8 (10) ***	26.4 ± 4.7 (10) *	19.5 ± 3.3 (12)	18.9 ± 5.7 (12) ***	22.1 ± 3.2 (13) *	40.0 ± 3.7 (8)
NO_3^-	0.8 ± 0.4 (7) ***	7.3 ± 2.1 (9)	12.8 ± 5.1 (11)	42.3 ± 17.2 (12) ***	23.6 ± 27.5 (7)	1.6 ± 1.6 (5)
SO_4^{2-}	0.9 ± 0.5 (10) ***	7.0 ± 2.3 (10) *	2.4 ± 0.6 (12)	10.1 ± 2.1 (12) ***	9.4 ± 1.0 (13) *	2.8 ± 0.4 (8)
Cl^-	0.5 ± 0.1 (8) ***	0.8 ± 0.2 (10) **	1.2 ± 0.2 (12)	6.3 ± 0.1 (12) ***	2.3 ± 0.2 (12) **	-
TZ^+	0.7 ± 0.1 (11)	0.6 ± 0.1 (10)	0.5 ± 0.1 (12)	1.2 ± 0.4 (12)	0.7 ± 0.4 (13)	0.6 ± 0.0 (6)
TZ^-	0.6 ± 0.1 (11)	0.7 ± 0.1 (10)	0.6 ± 0.1 (12)	1.4 ± 0.3 (12)	0.8 ± 0.4 (13)	0.7 ± 0.1 (6)
CBE	12.9 ± 7.7 (11)	-5.9 ± 6.8 (10)	-10.4 ± 5.8 (12)	-6.7 ± 10.5 (12)	-6.8 ± 3.1 (13)	-11.9 ± 7.3 (6)

TZ^+ = Ca + K+ Mg + Na (total cation charge); TZ^- = $HCO3^-$ + Cl^- + $SO4^{2-}$ + $NO3^-$ (total anion charge); CBE = (TZ^+ - TZ^-) / (TZ^+ + TZ^-) *x* 100, expressed in %.

Table S9. Biweekly solute fluxes [mg m^{-2} $15d^{-1}$]. Mean ± Standard Deviation (n =25). Means followed by *, **, *** indicate Mann-Whitney U-Test for significant differences by soil profile for same horizons (A and 2A only) at different significance levels ($p<0.05$, $p<0.01$, $p<0.001$).

Soil profile	CU-UR			TU-UP		
Horizon	A	2A	2BC	A	2A	3BC
Sampling depth [cm]	20	40	80	25	50	100
DOC	796.8 ± 644.2***	116.25 ± 77.67**	16.89 ± 9.92	60.20 ± 51.18***	60.48 ± 39.35**	71.09 ± 37.93
Fe	11.91 ± 5.0***	0.46 ± 0.36**	0.02 ± 0.01	0.22 ± 0.23***	0.20 ± 0.19**	0.18 ± 0.12
Al	28.34 ± 20.24***	1.69 ± 1.06	0.41 ± 0.32	1.03 ± 0.80***	1.25 ± 0.95	0.75 ± 0.43
K	137.31 ± 97.86***	8.02 ± 5.50	2.62 ± 2.16	31.27 ± 23.57***	28.59 ± 40.83	2.70 ± 1.61
Ca	77.48 ± 62.38***	54.59 ± 43.65*	14.88 ± 8.93	205.2 ± 142.9***	108.21 ± 84.63*	88.18 ± 84.63
Mg	13.30 ± 9.61***	17.87 ± 11.84**	10.27 ± 6.82	59.00 ± 38.97***	36.09 ± 29.52**	25.42 ± 14.14
Na	73.53 ± 51.59	77.06 ± 51.47	31.06 ± 18.47	91.72 ± 66.87	75.31 ± 57.79	97.31 ± 52.33
DSi	259.24 ± 206.70	292.68 ± 203.16	152.71 ± 102.47	288.50 ± 241.54	356.89 ± 285.26	354.61 ± 198.78
HCO_3^-	472.5 ± 219.60**	278.1 ± 128.50	125.07 ± 93.09	300.30 ± 277.70**	303.90 ± 208.30	812.68 ± 492.97
NO_3^-	14.78 ± 14.00***	86.99 ± 58.83	67.39 ± 33.31	639.0 ± 417.1***	3769.77 ± 7909.11	30.69 ± 45.08
SO_4^{2+}	12.58 ± 9.35***	81.17 ± 54.32*	12.95 ± 6.07	170.7 ± 133.3***	177.64 ± 133.32*	52.22 ± 28.48
Cl^-	7.92 ± 7.66***	9.10 ± 7.64***	6.72 ± 3.50	109.70 ± 87.01***	76.04 ± 87.78***	-

n= number of values

Table S10. Spearman correlation matrix of element concentrations [mg L^{-1}] in soil solutions grouped by soil profile

Element	Al	Fe	HCO_3^-	Ca	Mg	Na	DSi	K	NO_3^-	Cl^-	SO_4^{2+}
CU-UR											
DOC	0.90***	0.87***	0.64***	0.68***	-0.84***	-0.33**	-0.75***	0.90***	-0.75***	-0.79***	-0.42**
Al		0.90***	0.80***	0.62***	-0.71***	-0.26*	-0.70***	0.95***	-0.89***	-0.93***	-0.39**
Fe			0.69***	0.69***	-0.81***	-0.29*	-0.83***	0.87***	-0.88***	-0.71***	-0.39**
HCO_3^-				0.49***	-0.41**	0.06	-0.44**	0.79***	-0.72***	-0.78***	-0.03
Ca					-0.47***	0.08	-0.40**	0.62***	-0.47***	-0.39**	-0.03
Mg						0.60***	0.89***	-0.71***	0.83***	0.76***	0.52***
Na							0.46***	-0.28*	0.41**	0.27*	0.87***
DSi								-0.73***	0.83***	0.76***	0.45***
K									-0.87***	-0.90***	-0.41**
NO_3^-										0.90***	0.46***
Cl^-											0.38**
TU-UP											
DOC	-0.18	-0.44***	0.67***	-0.64***	-0.64***	-0.17	0.30**	-0.83***	-0.84***	-0.56***	-0.19
Al		-0.18	-0.65***	0.52***	0.52***	-0.33**	-0.09	0.37**	0.51***	-0.33*	0.81***
Fe			-0.05	0.11	0.05	-0.19*	-0.22*	0.39**	0.36**	0.18	-0.15
HCO_3^-				-0.85***	-0.86***	-0.08	0.26*	-0.81***	-0.81***	-0.55***	-0.66***
Ca					0.97***	0.26*	-0.41**	0.78***	0.69***	0.86***	0.65***
Mg						0.29*	-0.43***	0.80***	0.70***	0.86***	0.63***
Na							-0.28*	0.14	-0.03	0.82***	-0.22
DSi								-0.36**	-0.32**	-0.69***	-0.16
K									0.90***	0.68***	0.41**
NO_3^-										0.60***	0.50***
Cl^-											0.06

*, **, *** Significance levels (p-value < 0.05, < 0.01, < 0.001)

Table S11. Comparison of annual cation and Si fluxes [g m^{-2} y^{-1}] derived from soil solutions in this study with available reported solute fluxes in literature.

Site[a]	Vegetation type	Soil type	Ca	Mg	Na	K	DSi	T.Cat.	DOC	Reference
Jatunhuayco watershed, EC	Tussock grass (TU)	Andosols	2.20 - 5.13	0.64 - 1.48	1.88-2.43	0.07-0.78	7.21-8.92	14.2-16.9	1.5-1.8	This study
	Cushion plants (CU)		0.30 - 1.94	0.26 - 0.41	0.75-1.77	0.07-3.30	3.82-6.73	5.2-13.8	0.41-19.9	
Glacier Creek and Clear Creek, USA	Grassland prairie	Hapludolls, Hapludalfs	6.48	1.86	3.27	3.11	-	-		(Dere et al., 2019))
La Jara Creek, New Mexico, USA	Conifer forest	Alfisols, Mollisols	-	-	0.32	-	0.87	-	0.5-7.0	(McIntosh et al., 2017; Vázquez-Ortega et al., 2016))
Luquillo CZO, PR	Tropical mountains	Ultisols	-	0.31-1.53	-	-	3.5 - 11.2	-	-	(Buss et al., 2017))
Nagano, JP	Cold Temerate Forest	Andosols	-	-	-	-	-	-	0.9-1.1	(Fujii et al., 2011))
Klafastadir, IS	Grass and mosses	Andosols	-	-	-	-	-	-	2.4-8.4	(Sigfusson et al., 2006))
Western Iceland, IS	Non-forest soils	Andosols	0.00	0.24	0.23	0.20	1.12	1.80	-	(Guicharnaud and Paton, 2006))
Merced terraces, California, USA	Grasslands	Haploxeralf, Durixeralf	8.82	3.40	9.70	0.98	27.2	50.1	-	(White et al., 2005, p.white))
Hawaiian Islands, USA	Tropical forest	Hapludand, Udivitrand, Hydrudand, Kandiudox	0.10-10.0	-	-	0.03-1.32	1.2 - 26.3	-	-	(Hedin et al., 2003)
Rio Icacos watershed, PR	Tropical forest	-	4.11	1.63	3.10	1.36	12.2	22.4	-	(White et al., 1998))
Loch Vale, Rocky Mountains, USA*	Alpine tundra	Cryochrept	1.62	0.78	0.35	0.68	0.04	3.47	-	(Clow and Drever, 1996)

Abbreviations: Mean annual precipitation (MAP), Mean annual temperature (MAT)
A Site: EC = Ecuador, USA = United States of America, PR = Puerto Rico, JP = Japan, IS = Iceland
* Average fluxes for the summer period
¥ Seasonal ranges

Figure S1. Linear regressions between biweekly water flux and solute concentrations.

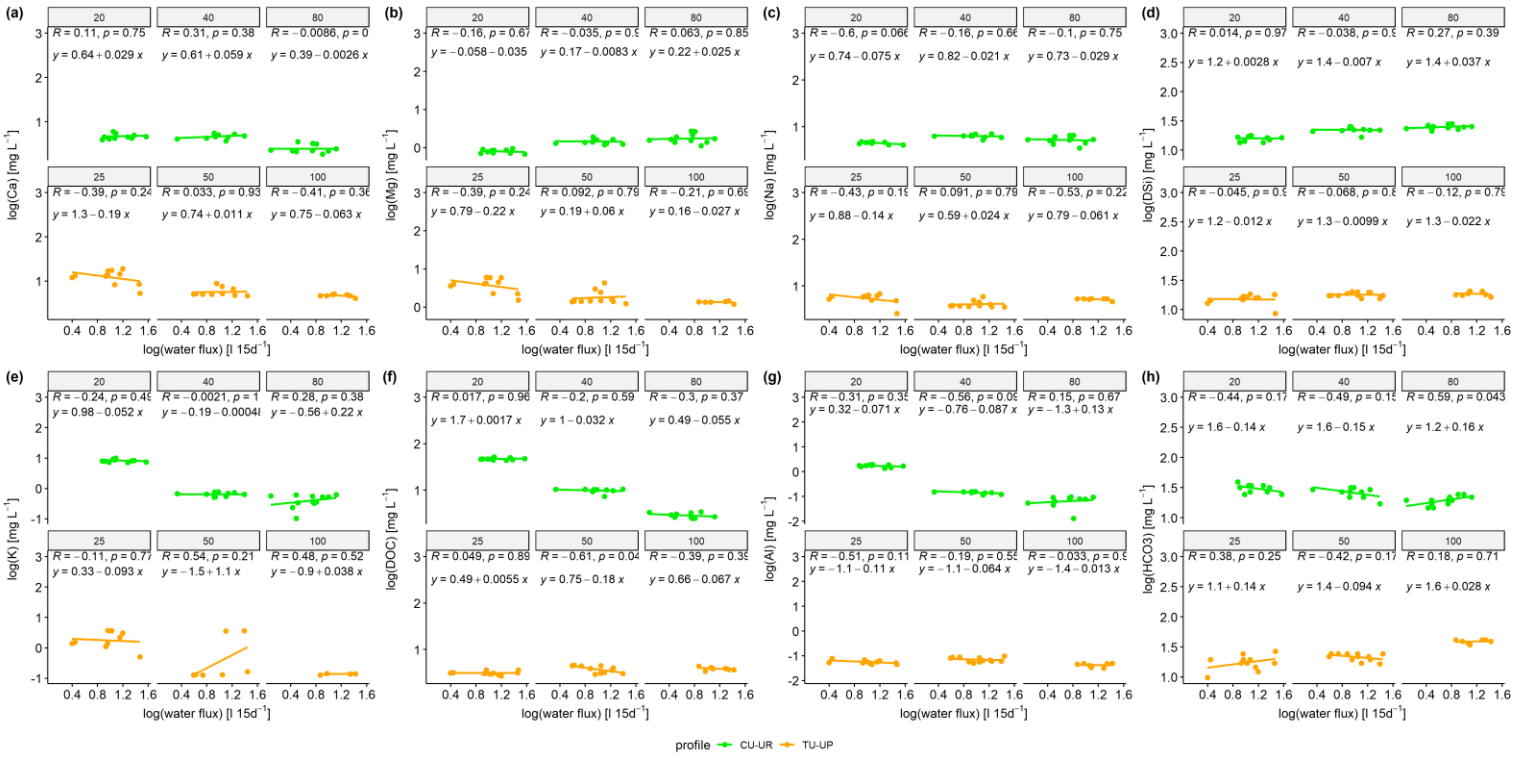

Figure S2. Determination of dry, intermediate, and wet months based on monthly rainfall for each soil profile. The upper and lower dotted lines represent the 75th and 25th percentiles, respectively. The intermediate dashed line represents the mean annual rainfall. Dry (wet) months are represented below 25th (above 75th) percentile.

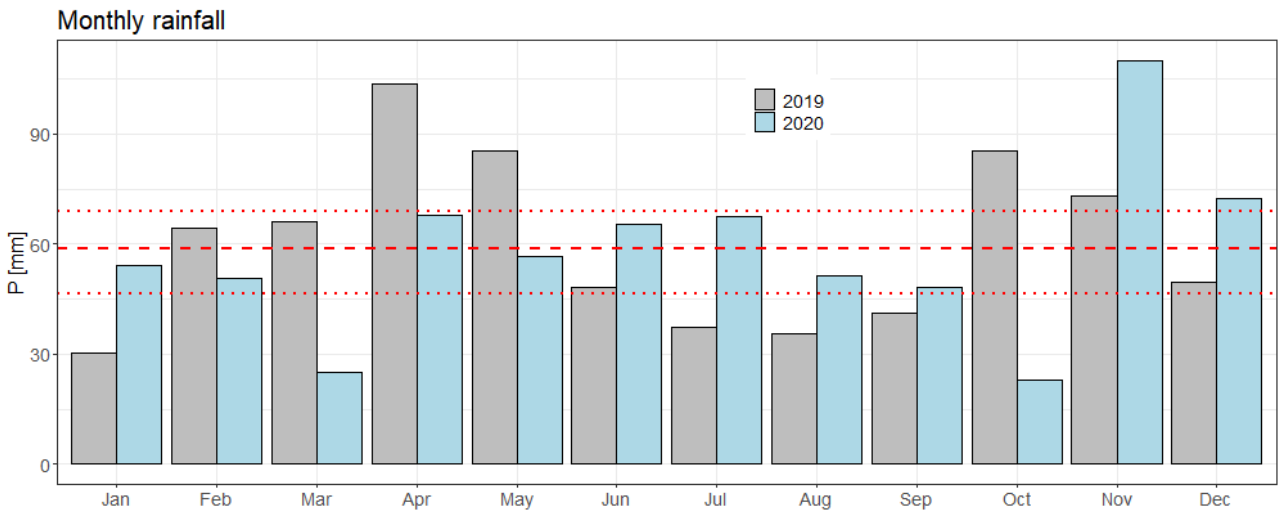

Figure S3. Soil properties along with depth (a) water retention at saturation (θ_{SAT}), (b) water retention at field capacity (θ_{FC}), (c) water retention at wilting point (θ_{WP}), (d) sand content, (e) silt content, and (f) clay content.

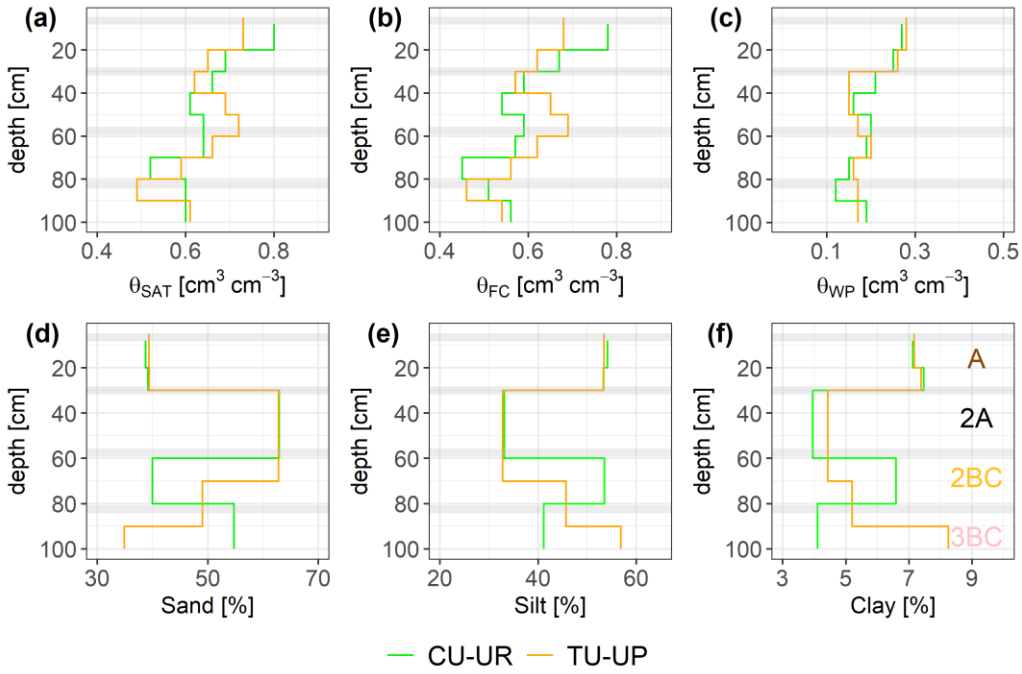

Figure S4. Biweekly solute concentrations (Fe, NO_3^-, Cl^-, SO_4^{2-}) for both soil profiles. The Mann-Whitney U test was applied for differences between vegetation types, with levels of significance *, **, *** corresponding to $p<0.05$, $p<0.01$, $p<0.001$.

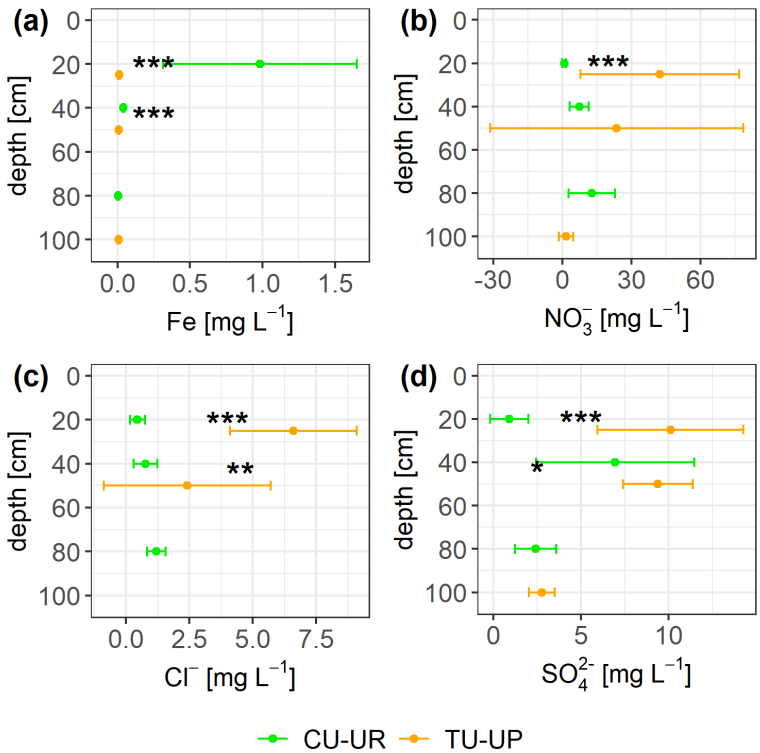

Figure S5. Annual solute fluxes for the studied soil profiles

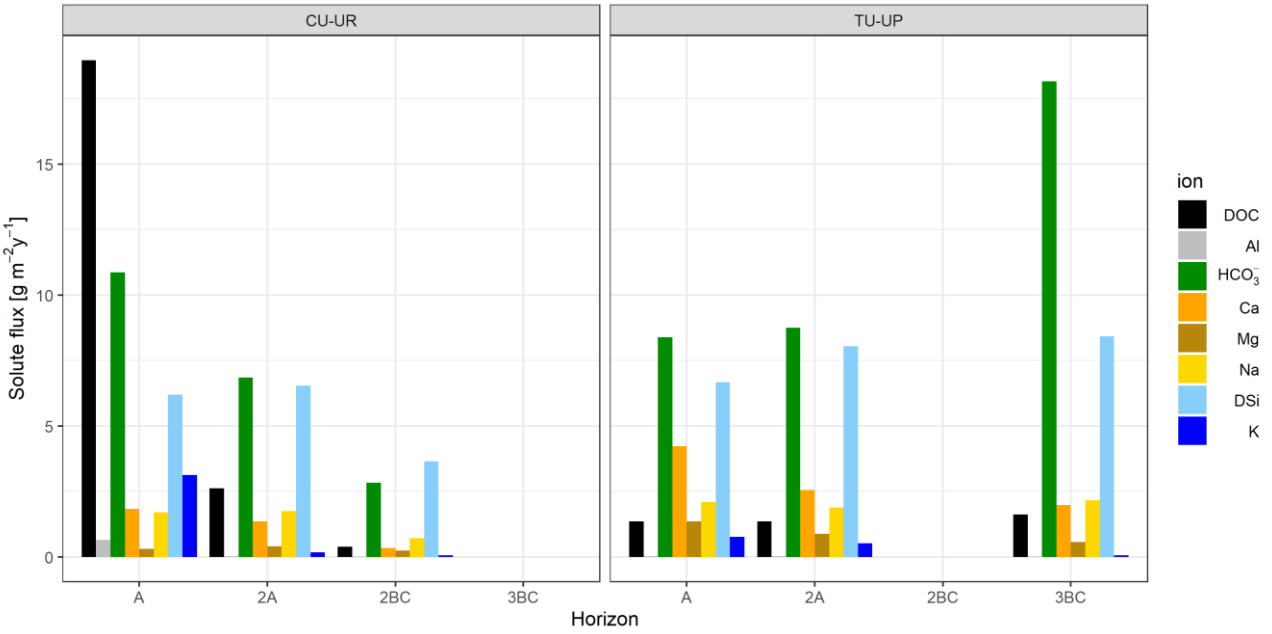

Figure S6. Daily meteorological variables (rainfall, air temperature, relative humidity) recorded at the soil profiles (a-c) as well as meteorological variables (solar radiation and wind speed) recorded by the automatic weather station JTU_AWS (d-e). Red (blue) stripes represent months defined as dry (wet) periods.

Figure S7. Simulated and observed volumetric water content (VWC) for TU-UP considering lower interception loss (55.8% Calamagrostis coverage) adapted from Ochoa-Sanchez et al., 2018. The vertical dashed line separates calibration and validation periods. Horizontal dashed lines indicate filed capacity at corresponding soil moisture sensor depth.

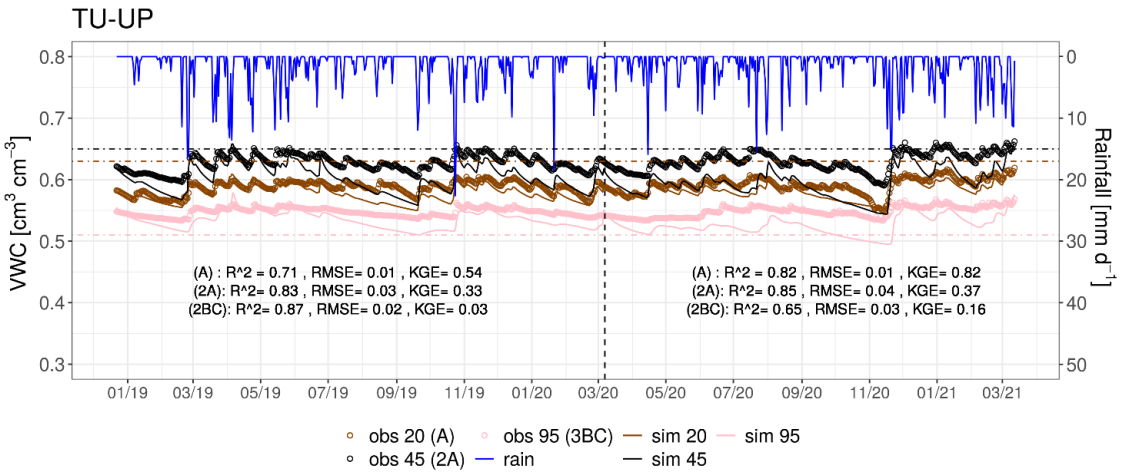

Figure S8. Water retention curves (matric potential vs. volumetric water content) plotted per horizon and soil profile, with CU-UR plotted in green and TU-UP plotted in orange. Two to three replica samples were analyzed per horizon and per profile.

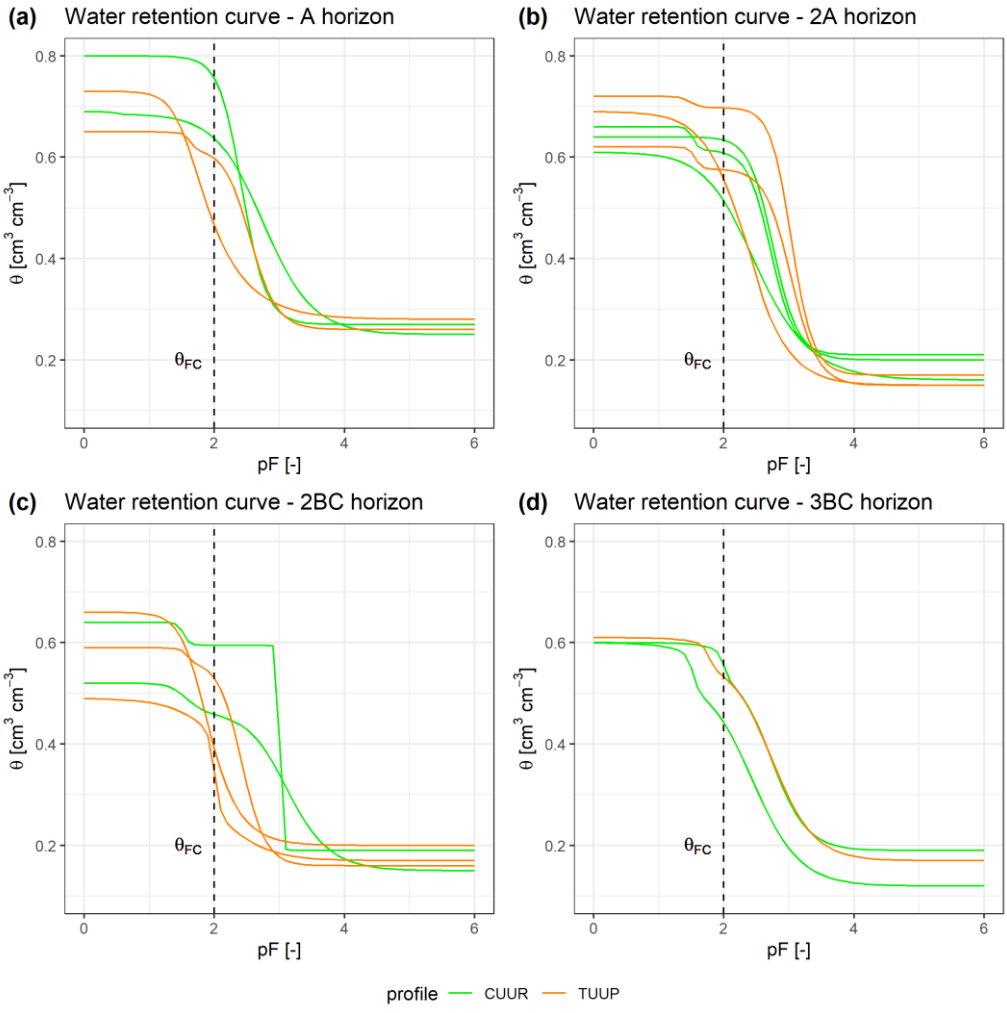

Figure S9. Hydraulic conductivity curve (matric potential vs. hydraulic conductivity) plotted per horizon and soil profile, with CU-UR plotted in green and TU-UP plotted in orange. Two to three replica samples were analyzed per horizon and per profile.

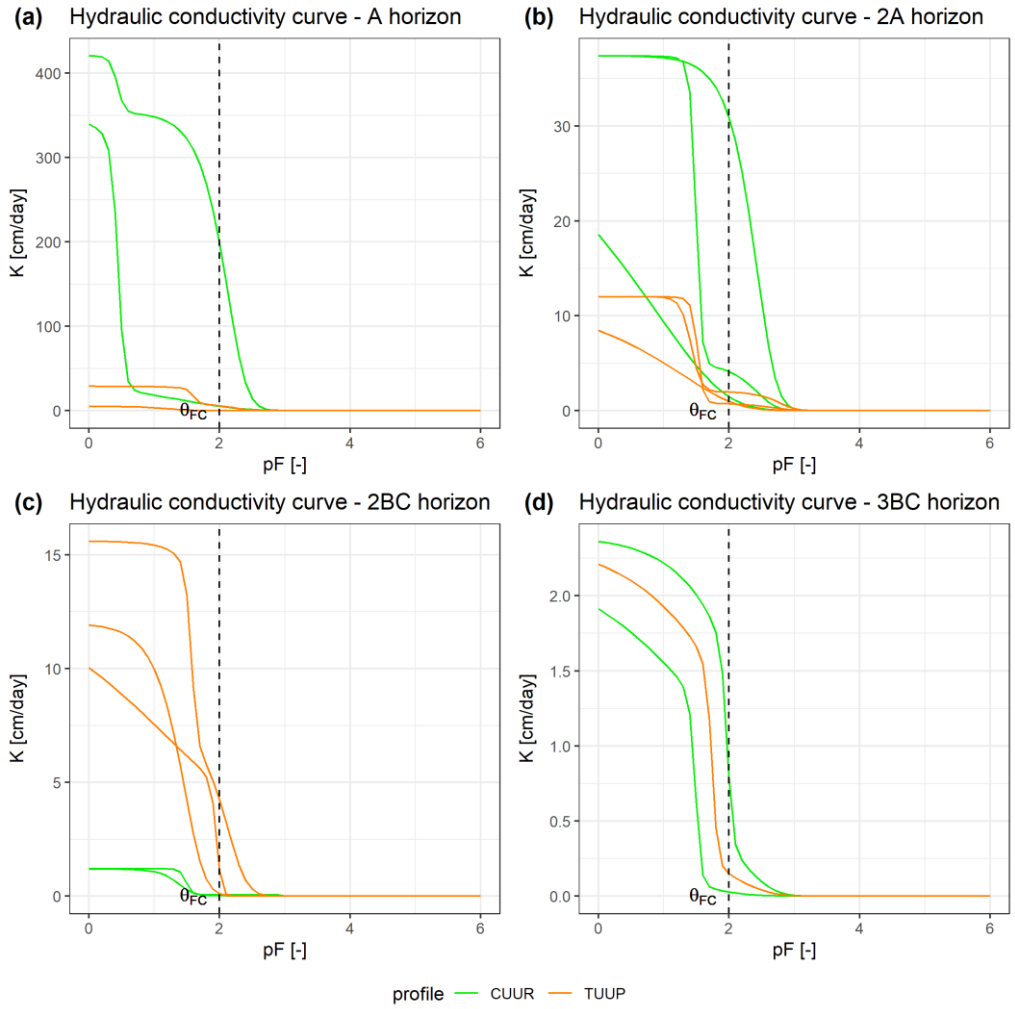

Section S2

Calibration water content reflectometers

Calibration of water content reflectometers (CS650, Campbell Scientific) was performed by simultaneously measuring permittivity and volumetric water content on large undisturbed soil samples (diameter = 40, height = 30 cm) collected in the field with PVC tubes (TIGRE Ecuador). These samples were saturated via capillarity rise, in the LEMSUR Laboratory at Escuela Politécnica Nacional in Quito. Sensors were introduced into the samples, connected to a data logger (CR300, Campbell Scientific); Then the samples were left to dry out while periodically extracting three subsamples (diameter = ~3 cm, height = ~7 cm) from which volumetric water content was determined. Five calibration equations ($R^2 \geq 0.94$) were derived by relating permittivity to volumetric water content. Independent validation of the calibration curves was performed on undisturbed samples (100 cm^3) taken in the field during the monitoring period (Figure 1). The equation for 2BC and 3BC horizons was fitted to field validation measurements and validated with laboratory data.

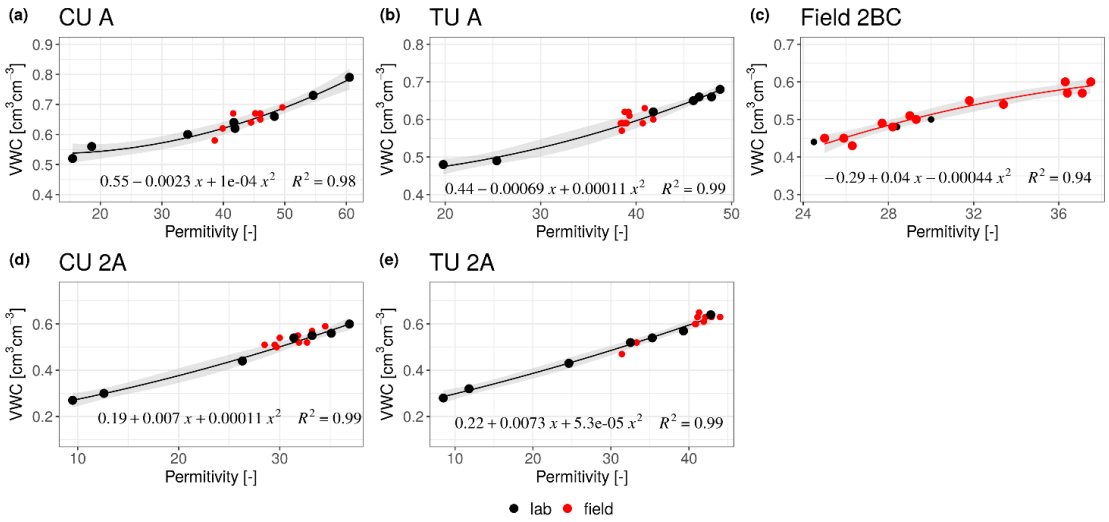

Figure S10. Calibration curve for soil moisture sensors

Table S12. Calibration equations of water content reflectometers

Soil profile	Sensor	Horizon	Depth [cm]	Calibration Equation[1]	R^2
CU-UPR	Water content reflectometer	A	20	0.55 -0.0023x +0.0001x^2	0.98
		2A	40	0.19 +0.007x +0.00011x^2	0.99
		2BC/3BC	80	-0.29 +0.04x -0.00044x^2 *	0.94
TU-UP	Water content reflectometer	A	25	0.44 -0.00069x +0.00011x^2	0.99
		2A	45	0.22 +0.0073x +0.000053x^2	0.99
		3BC	95	-0.29 +0.04x -0.00044x^2 *	0.94

[1] x is permittivity recorded from water content reflectometers, * Equation fitted to field measurements

Section S3

Soil water model

1. Governing equations and model set-up

The model performs water movement, solutes and heat in variably-saturated rigid porous medium. The code solves the Richards Equation (Richards, 1931) assuming negligible effects of the vapor phase on the water mass balance, and of water flow due to thermal gradients. The Richards Equation for vertical flow is the following:

$$\frac{\partial \theta}{\partial t} = \frac{\partial}{\partial x}\left[K(h)\left(\frac{\partial h}{\partial x} + 1\right)\right] \quad (1)$$

where, θ is the volumetric water content [$cm^3\ cm^{-3}$], *h* is the matric head [cm], *t* is time [day], *x* is the spatial coordinate, upward positive [cm], *K(h)* is the unsaturated hydraulic conductivity [$cm\ day^{-1}$]. Eq. (1) can be solved defining the soil hydraulic functions as well as providing boundary and initial conditions. In order to provide the initial soil hydraulic function parameters two approaches of water retention functions were explored. First, the unimodal van Genuchten function (van Genuchten, 1980) and second, the bimodal van Genuchten function (Durner, 1994), which considers the porous medium as the overlapping of unimodal van Genuchten functions. As the second approach reduced the root mean squared error in the fitting in comparison to the unimodal, the bimodal approach was chosen, and initial parameter values and ranges were introduced (Table S4).

Following the bimodal approach (Durner, 1994), it combines two unimodal van Genuchten models that are weighted by a factor, ω, to represent the entire pore system as the combination of matrix (M) and structure (S) pore systems. The equations for the water retention curve can be described by estimating the soil water content (θ) as a function of matric potential head (h) as follows:

$$\theta = \theta_r + \omega_M \frac{\theta_{Bs} - \theta_r}{[1 + (\alpha_M\, h)^{n_M}]^{m_M}} + \omega_S \frac{\theta_{Bs} - \theta_r}{[1 + (\alpha_S\, h)^{n_S}]^{m_S}} \quad (2)$$

$$m = 1 - \frac{1}{n} \quad (3)$$

$$\omega_M + \omega_S = 1 \quad (4)$$

Where θr is the residual water content at -1500 kPa (cm3 cm-3); θBS is the bulk water content at saturation (cm3 cm-3); h is the matric potential head (cm); α (cm-1), n (-) and m (-) represent curve-shape fitting parameters; the underscripts M and S represent the matrix and structure pore domains, respectively.

The following equation details the bimodal unsaturated hydraulic conductivity (Reynolds, 2017):

$$K_B(h) = K_{B_{SAT}}\left(\sum_{i=1}^{2} \omega_i [1 + (\alpha_i h)^{n_i}]^{-m_i}\right)^{\tau} \left(\frac{\sum_{i=1}^{2} \omega_i \alpha_i \{1 - (\alpha_i h)^{(n_i - 1)}[1 + (\alpha_i h)^{n_i}]^{-m_i}\}}{\sum_{i=1}^{2} \omega_i \alpha_i}\right)^2 \quad (5)$$

where, $K_{B\ SAT}$ [$cm\ day^{-1}$] is the saturated hydraulic conductivity of the bulk medium, i=1,2 refers to the structure and matrix domain and τ is the macroscopic tortuosity of the conductivity (assigned to 0.5 as suggested by Mualem, (1976) for mineral soils and corroborated by Dettmann et al., (2014) for soils with organic carbon content ≤ 18%)

The soil profiles were represented from the A to the 3BC horizons and discretized with a 2 mm resolution mesh. The models were constructed with nine layers according the spatial discretization of the soil hydraulic properties. Observational nodes were distributed in consonance with the location of water content reflectometers and for each soil layer. The upper boundary condition was set to "atmospheric boundary with surface runoff" and the lower boundary was set as "free drainage". The former was represented by the daily rainfall and the calculated potential evapotranspiration (ETp) based on the Penman-Montheith equation, based on measured variables from the JTU_AWS automatic weather

station. The latter was defined based on the observation of no water table at topographical summit positions. The initial conditions were set to pressure heads and obtained in the basis of the observed soil moisture and the water retention function. The model was set to run at daily basis for two separated time periods: (i) calibration between 22/12/2018 – 05/03/2020, and (ii) validation between 06/03/2020 – 12/03/2021.

2. Sensitivity analysis

Based on the number of layers as well as on the soil hydraulic functions a total of 72 parameters were suited for calibration per soil profile. Therefore, in order to reduce the number of soil hydraulic parameters we performed a global sensitivity analysis (GSA) using the variance-based Sobol method (Sobol, 2001). This method quantifies the variance contributed by each parameter to the variance of the model output. The variance amount was represented by the first-order (S_i) and total effect (S_T) Sobol's sensitivity indices. The first-order represent the contribution of a certain parameter to the model output variance; whereas the total effect indicates the interactions of a certain parameter with the rest (Brunetti et al., 2016). Due to the nature of non-linearity of soil water models, the Monte Carlo approach was applied to calculate the variances based on $n \cdot (p+2)$ model evaluations, where n is the number of samples, and p is the number of parameters (Jansen, 1999; Saltelli et al., 2010). However, a revision for hydrological models found that for the Sobol method the number of model evaluations rarely exceeds 100,000 (Song et al., 2015), and a recent study corroborates this number (Brunetti et al., 2016). Therefore, we used $n = 1500$, giving a total of 111,000 model runs for each soil profile.
The sensitivity analysis was performed using the R programming language, and in particular the "sensitivity" package (Ioos et al., 2021). An R script creates a new input file and overwrites the soil hydraulic parameters at all layers at each iteration, based on random samples (X1 and X2) generated from uniformly distributed soil hydraulic parameters between ranges (Table S4). These ranges were based on observed and theoretical values for similar soils (Dettmann et al., 2014). These parameters values then are executed as forward numerical modelling in the HRYUS code. Then Kling-Gupta efficiency (KGE; Gupta et al., 2009) objective function was calculated for each iteration for the observed soil moisture at three depths. HYDRUS-1D skipped non-convergent runs after 30 s and attributed them a large negative value (-1^10) to the objective function. The resulting values of the objective function along with the random samples were further use to calculate the Sobol's indices. The most sensitive parameters were considered when their indices corresponding to the first-order (S_i) and the total effect (S_T) were higher than 5% and 25% of model output variance, respectively.

3. Model calibration and independent validation

Once sensitive parameters have been identified by Sobol method, an inverse numerical modelling was conducted based on the mean observed soil hydraulic properties (θ_S, θ_r, K_{SAT}) and the fitted parameters (α, n, α_2, n_2, w_2) from the bimodal van Genuchten water retention functions (Table S4). The inverse modelling optimized the sensitive soil hydraulic parameters based on the soil volumetric water content at the three respective depths by using the Marquardt-Levenberg algorithm (Šimůnek and Hopmans, 2002) and the default objective function (Šimůnek et al., 2018). The optimization was performed for the calibration period by minimizing the objective function sum of the squared differences between observed and simulated soil moisture at each depth. The goodness of fit was assessed by the different measures, for instance the coefficient of determination (R^2), the root mean square error (RMSE) and the Kling-Gupta efficiency (KGE). The optimized set of parameters were then applied for a direct forward modeling in HYDRUS for the validation period, in order to demonstrate the ability of the model to reproduce the same processes with an independent data series. The validation period was also evaluated with the same measures of goodness of fit. Both calibration and validation periods consisted in at least one hydrological year covering dry and wet conditions.

4. Sensitivity analysis results

The outcome of the Sobol method showed that contribution of the soil hydraulic parameters to the variance of the output model was similar for most parameters, except by few most sensitive parameters (Table S5). For the cushion plant profile, most sensitive soil hydraulic parameters (6) are n along depth; whereas for tussock profile the most sensitive parameters (7) were related to the soil hydraulic properties of the uppermost depth (15 cm). The calibrated soil hydraulic parameters by inverse modelling differed for each soil profile (Table S6). Following the results from the sensitivity analysis, for the cushion plant profile, n parameters at most depths were fitted, except at 75cm; whereas for tussock grass profile most fitted soil hydraulic parameters corresponded to the upper most soil layer (15 cm) as well as the α and n parameters at lower depths (60-80 cm). The small standard error for most parameter values indicate that the inverse approach gave in general stable fitted estimates. Mass balance error of the model accounted for less than 0.75% for both profiles.

Section S4

Interception analysis

The interception analysis started with the definition of the separation time between rainfall events, which in literature can be found between 4 and 6 hours for paramo ecosystems (Ochoa-Sánchez et al., 2018; Tenelanda-Patiño et al., 2018). From our analyses, we found that a separation time of 5 hours produces 568 events with a maximum duration of 54 hours. This has a similar number of events to 6 hours (553) but a shorter maximum rainfall duration (74 hours).

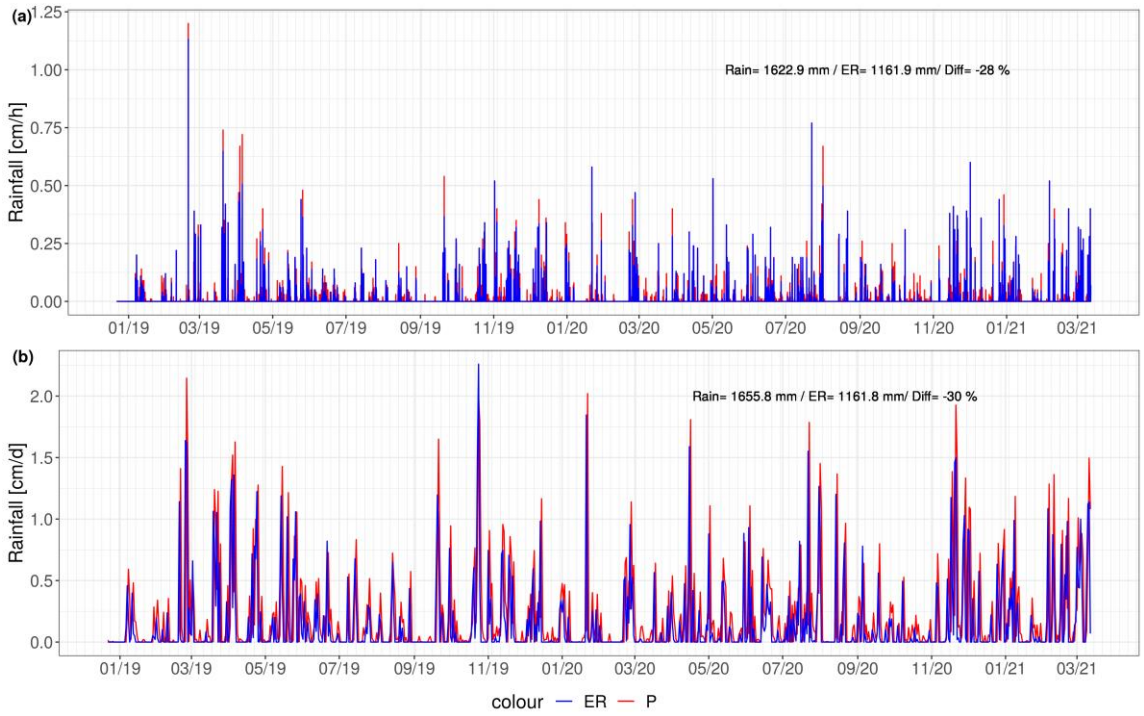

Figure S11. Event separation for 5 hours interval time (a) for hourly rainfall and (b) for daily rainfall. ER means effective rainfall and P original rainfall.

We adapt the method described by Ochoa-Sánchez et al., (2018) to represent a coverage area of 55.8%, however it could be reach even 33% of coverage. Based on 55.8% tussock coverage, vegetation storage reduced to 0.95 mm; whereas in other sites storage in grassland vegetation vary from 0.13 to 0.8 mm (Ochoa- Sánchez et al., 2018). From our data 257 events fell in the range below 0.95 mm and were converted to 0 mm rainfall, as considered to be stored completely at the vegetation canopy. For the remaining events (296), the interception loss was calculated according to the equation developed and further multiplied by the 55.8% corresponding to the vegetation coverage. In other grassland sites, rainfall interception has been reported to vary from 5 to 40 %. This reduction was mainly attributed to vegetation characteristics (shorter stature grasses, partial bare soil coverage) and climatic conditions (Ochoa- Sánchez et al., 2018).
The effective rainfall reduced 30 % in comparison to original rainfall. Once this effective rainfall was used to force the HYDRUS model, the results indicate a significant reduction in simulated soil water content, especially during the drier season for small rainfall events (< 0.95 mm), for the lower horizons (2A and 3BC). This reduction in soil water content cannot be further compensated during rainy season.

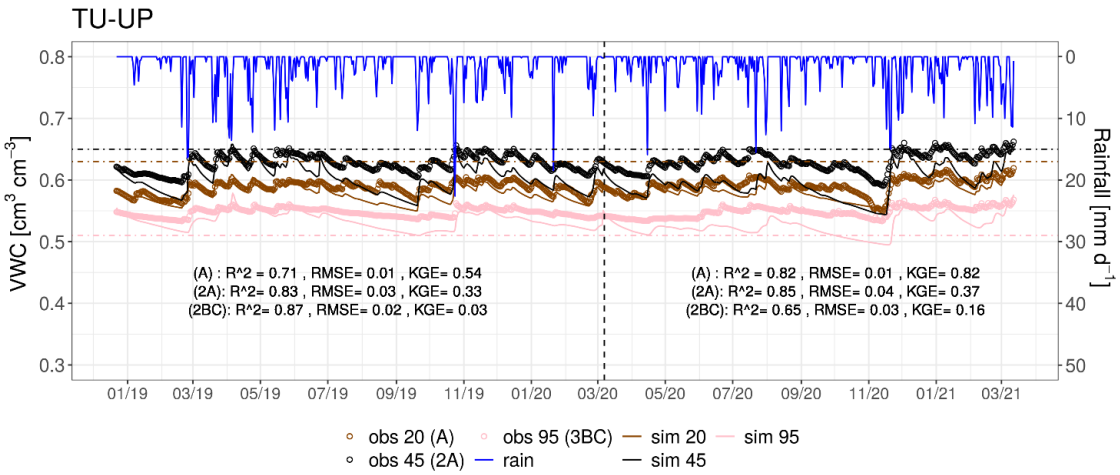

Figure S12. Simulated and observed volumetric water content (VWC) by HYDRUS 1-D model for TU-UP considering interception adapted (55.8% *Calamagrostis* coverage) from Ochoa-Sanchez et al., 2018. Vertical dashed line separates calibration and validation periods. Horizontal dashed lines indicate filed capacity at corresponding soil moisture sensor depth.

When we further compare to the observed fluxes with observed water fluxes from fluxmeter in the 2A horizon. The results indicate general reduction in simulated water fluxes. However, a drastic reduction in simulated water flux is evident after the drier period July-August 2019.

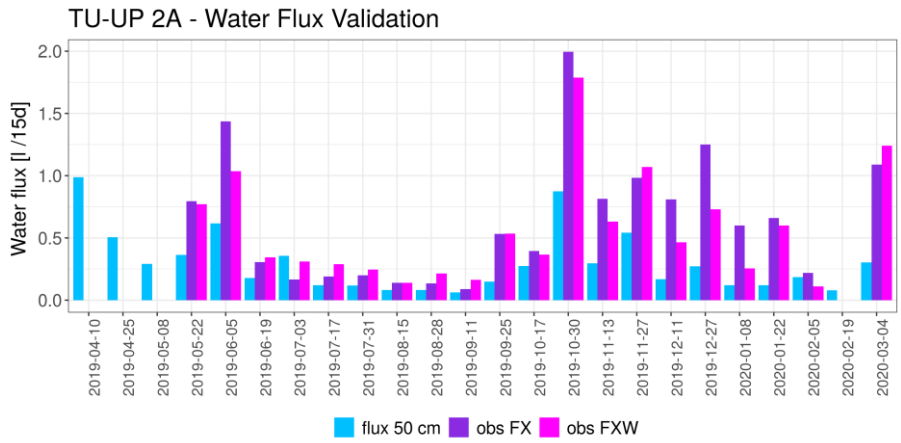

Figure S13. Measured water flux at 2A horizon versus simulated flux considering 55.8% tussock coverage.

References

Brunetti, G., Šimůnek, J., and Piro, P.: A comprehensive numerical analysis of the hydraulic behavior of a permeable pavement, Journal of Hydrology, 540, 1146–1161, https://doi.org/10.1016/j.jhydrol.2016.07.030, 2016.

Buss, H. L., Chapela Lara, M., Moore, O. W., Kurtz, A. C., Schulz, M. S., and White, A. F.: Lithological influences on contemporary and long-term regolith weathering at the Luquillo Critical Zone Observatory, Geochimica et Cosmochimica Acta, 196, 224–251, https://doi.org/10.1016/j.gca.2016.09.038, 2017.

Clow, D. W. and Drever, J. I.: Weathering rates as a function of flow through an alpine soil, Chemical Geology, 132, 131–141, https://doi.org/10.1016/S0009-2541(96)00048-4, 1996.

Dere, A. L., Miller, A. W., Hemje, A. M., Parcher, S. K., Capalli, C. A., and Bettis, E. A.: Solute Fluxes Through Restored Prairie and Intensively Managed Critical Zones in Nebraska and Iowa, Front. Earth Sci., 7, 24, https://doi.org/10.3389/feart.2019.00024, 2019.

Dettmann, U., Bechtold, M., Frahm, E., and Tiemeyer, B.: On the applicability of unimodal and bimodal van Genuchten–Mualem based models to peat and other organic soils under evaporation conditions, Journal of Hydrology, 515, 103–115, https://doi.org/10.1016/j.jhydrol.2014.04.047, 2014.

Durner, W.: Hydraulic conductivity estimation for soils with heterogeneous pore structure, Water Resour. Res., 30, 211–223, https://doi.org/10.1029/93WR02676, 1994.

Fujii, K., Funakawa, S., Shinjo, H., Hayakawa, C., Mori, K., and Kosaki, T.: Fluxes of dissolved organic carbon and nitrogen throughout Andisol, Spodosol and Inceptisol profiles under forest in Japan, Soil Science and Plant Nutrition, 57, 855–866, https://doi.org/10.1080/00380768.2011.637304, 2011.

van Genuchten, M. Th.: A Closed-form Equation for Predicting the Hydraulic Conductivity of Unsaturated Soils, Soil Science Society of America Journal, 44, 892–898, https://doi.org/10.2136/sssaj1980.03615995004400050002x, 1980.

Guicharnaud, R. and Paton, G. I.: An evaluation of acid deposition on cation leaching and weathering rates of an Andosol and a Cambisol, Journal of Geochemical Exploration, 88, 279–283, https://doi.org/10.1016/j.gexplo.2005.08.056, 2006.

Gupta, H. V., Kling, H., Yilmaz, K. K., and Martinez, G. F.: Decomposition of the mean squared error and NSE performance criteria: Implications for improving hydrological modelling, Journal of Hydrology, 377, 80–91, https://doi.org/10.1016/j.jhydrol.2009.08.003, 2009.

Hedin, L. O., Vitousek, P. M., and Matson, P. A.: Nutrient Losses over four million years of tropical forest development, Ecology, 84, 2231–2255, https://doi.org/10.1890/02-4066, 2003.

Ioos, M., et al, and et al: Global Sensitivity Analysis of Model Outputs Package 'sensitivity,' 2021.

Jansen, M. J. W.: Analysis of variance designs for model output, Computer Physics Communications, 117, 35–43, https://doi.org/10.1016/S0010-4655(98)00154-4, 1999.

McIntosh, J. C., Schaumberg, C., Perdrial, J., Harpold, A., Vázquez-Ortega, A., Rasmussen, C., Vinson, D., Zapata-Rios, X., Brooks, P. D., Meixner, T., Pelletier, J., Derry, L., and Chorover, J.: Geochemical evolution of the Critical Zone across variable time scales informs concentration-discharge relationships: Jemez River Basin Critical Zone Observatory, Water Resour. Res., 53, 4169–4196, https://doi.org/10.1002/2016WR019712, 2017.

Mualem, Y.: A new model for predicting the hydraulic conductivity of unsaturated porous media, Water Resour. Res., 12, 513–522, https://doi.org/10.1029/WR012i003p00513, 1976.

Ochoa-Sánchez, A., Crespo, P., and Célleri, R.: Quantification of rainfall interception in the high Andean tussock grasslands, Ecohydrology, 11, 11, https://doi.org/10.1002/eco.1946, 2018.

Reynolds, W. D.: Use of bimodal hydraulic property relationships to characterize soil physical quality, Geoderma, 294, 38–49, https://doi.org/10.1016/j.geoderma.2017.01.035, 2017.

Richards, L. A.: Capillary conduction of liquids through porous mediums, Physics, 1, 318–333, https://doi.org/10.1063/1.1745010, 1931.

Saltelli, A., Annoni, P., Azzini, I., Campolongo, F., Ratto, M., and Tarantola, S.: Variance based sensitivity analysis of model output. Design and estimator for the total sensitivity index, Computer Physics Communications, 181, 259–270, https://doi.org/10.1016/j.cpc.2009.09.018, 2010.

Sigfusson, B., Paton, G. I., and Gislason, S. R.: The impact of sampling techniques on soil pore water carbon measurements of an Icelandic Histic Andosol, Science of The Total Environment, 369, 203–219, https://doi.org/10.1016/j.scitotenv.2006.01.012, 2006.

Šimůnek, J. and Hopmans, J. W.: Parameter Optimization and Nonlinear Fitting, in: SSSA Book Series, edited by: Dane, J. H. and Clarke Topp, G., Soil Science Society of America, Madison, WI, USA, 139–157, https://doi.org/10.2136/sssabookser5.4.c7, 2002.

Šimůnek, J., Šejna, M., Saito, H., Sakai, M., and van Genuchten, M. Th.: The HYDRUS-1D Software Package for Simulating the Movement of Water, Heat, and Multiple Solutes in Variably Saturated Media, Department of Environmental Sciences, University of California Riverside, Riverside, Riverside, California, USA, 348 pp., 2018.

Sobol, I. M.: Global sensitivity indices for nonlinear mathematical models and their Monte Carlo estimates, Mathematics and Computers in Simulation, 55, 271–280, https://doi.org/10.1016/S0378-4754(00)00270-6, 2001.

Song, X., Zhang, J., Zhan, C., Xuan, Y., Ye, M., and Xu, C.: Global sensitivity analysis in hydrological modeling: Review of concepts, methods, theoretical framework, and applications, Journal of Hydrology, 523, 739–757, https://doi.org/10.1016/j.jhydrol.2015.02.013, 2015.

Tenelanda-Patiño, D., Crespo-Sánchez, P., and Mosquera-Rojas, G.: Umbrales en la respuesta de humedad del suelo a condiciones meteorológicas en una ladera Altoandina, MSKN, 9, 53–65, https://doi.org/10.18537/mskn.09.02.07, 2018.

Vázquez-Ortega, A., Huckle, D., Perdrial, J., Amistadi, M. K., Durcik, M., Rasmussen, C., McIntosh, J., and Chorover, J.: Solid-phase redistribution of rare earth elements in hillslope pedons subjected to different hydrologic fluxes, Chemical Geology, 426, 1–18, https://doi.org/10.1016/j.chemgeo.2016.01.001, 2016.

White, A. F., Blum, A. E., Schulz, M. S., Vivit, D. V., Stonestrom, D. A., Larsen, M., Murphy, S. F., and Eberl, D.: Chemical Weathering in a Tropical Watershed, Luquillo Mountains, Puerto Rico: I. Long-Term Versus Short-Term Weathering Fluxes, Geochimica et Cosmochimica Acta, 62, 209–226, https://doi.org/10.1016/S0016-7037(97)00335-9, 1998.

White, A. F., Schulz, M. S., Vivit, D. V., Blum, A. E., Stonestrom, D. A., and Harden, J. W.: Chemical weathering rates of a soil chronosequence on granitic alluvium: III. Hydrochemical evolution and contemporary solute fluxes and rates, Geochimica et Cosmochimica Acta, 69, 1975–1996, https://doi.org/10.1016/j.gca.2004.10.003, 2005.